Electric interface condition for sliding and viscous contacts

J. Rekier,[1,2,*] S. A. Triana,[1] A. Trinh,[3] and B. Buffett[2]
[1]*Royal Observatory of Belgium, 3 avenue circulaire, B-1180 Brussels, Belgium*
[2]*Department of Earth and Planetary Science, University of California, Berkeley, California 94720, USA*
[3]*Lunar and Planetary Lab, University of Arizona, Tucson, Arizona 85721-0092, USA*

(Received 2 March 2023; accepted 9 June 2023; published 14 July 2023)

The first principles of electromagnetism impose that the tangential electric field must be continuous at the interface between two media. The definition of the electric field depends on the frame of reference, leading to an ambiguity in the mathematical expression of the continuity condition when the two sides of the interface do not share the same rest frame. We briefly review the arguments supporting each choice of interface condition and illustrate how the most theoretically consistent choice leads to a paradox in induction experiments. We then present a model of sliding contact between two solids and between a fluid and a solid and show how this paradox can be lifted by taking into account the shear induced by the differential motion in a thin intermediate viscous layer at the interface, thereby also lifting the ambiguity in the electric interface condition. We present some guidelines regarding the appropriate interface condition to employ in magnetohydrodynamics applications, in particular for numerical simulations in which sliding contact is used as an approximation of the viscous interface between a conducting solid and a fluid of very low viscosity such as in planetary interior simulations.

DOI: 10.1103/PhysRevResearch.5.033029

I. INTRODUCTION

Solving problems of electromagnetism in continuous media requires imposing continuity conditions at interfaces between regions with different properties. These interface conditions can be derived axiomatically from Maxwell's equations in the integral form (e.g., [1,2]). From the same starting point, one can derive Maxwell's equations in their differential *local* form by making use of the divergence and curl theorems. Some textbooks prefer to work backward from there and attempt to derive interface conditions by integrating the differential Maxwell equations across the interface (e.g., [3]). While this is perfectly fine in most situations, it leads to difficulties when the two sides of the interface are not at rest with respect to each other. Such a situation occurs in deforming media for which careful inspection of Maxwell's equations in their "material form" shows that it is the tangential electric field measured in the instantaneous rest frame—equivalent to the *electromotive force* per unit length—on each side of the interface that must be continuous [4] (see also [5,6]). This condition is relevant to electroelastic applications [7]. It is also the one commonly used in plasma physics [8–10] (see also [11]).

Recently, Satapathy and Hsieh [12] used two rail gun experiments to confirm the validity of that condition at the interface between two solids in sliding contact. They showed that the commonly used alternative interface condition, which imposes that the tangential electric field measured *in the laboratory frame* is continuous, failed to reproduce experimental data. This result is in contrast to those of other classical experiments, in which the latter was found to be valid (e.g., [13]). The present paper proposes to address this tension.

In Sec. II we state the problem in the mathematical form and briefly review the arguments in favor of both interface conditions. We also illustrate how the more theoretically consistent choice of boundary condition leads to a paradox in a simple rotating cylinder induction experiment. In Sec. III we introduce a simple model of interface and show how the paradox is lifted when one takes into account the role of shears in an intermediate viscous layer between the two media. Finally, in Sec. IV we extend the model to the case of a solid-fluid interface and show how the fluid boundary layer naturally serves the role of an intermediate layer in that case. We present some conclusions and guidelines pertaining to magnetohydrodynamics applications and numerical simulations in Sec. V.

II. THEORETICAL MOTIVATION

In this section, we review the electric boundary condition between two media from a theoretical point of view. We then illustrate its different interpretations using a simple example.

A. Electric boundary condition

At the interface between two media, the electric field $\mathbf{E}$ satisfies the following junction condition (e.g., [1,2]):

$$\hat{\mathbf{n}} \times [\mathbf{E}]_{-}^{+} = \mathbf{0}, \tag{1}$$

where the notation $[\cdot]_{-}^{+}$ denotes the jump in the quantity in brackets across the interface with unit normal vector $\hat{\mathbf{n}}$. Equation (1) is ambiguous as long as one does not specify the frame of reference. Indeed, in the nonrelativistic limit, the

*Corresponding author: jeremy.rekier@observatory.be

TABLE I. Interface conditions used throughout this work.

Label	Condition	Equivalent form	Eqs. in main text
CI	$\hat{\mathbf{n}} \times [\mathbf{E}]^+_- = \mathbf{0}$	$\hat{\mathbf{n}} \times [\eta\nabla \times \mathbf{B}]^+_- = (\hat{\mathbf{n}} \cdot \mathbf{B})[\mathbf{v}]^+_-$	Eqs. (1) and (4) with $\hat{\mathbf{n}} \cdot \mathbf{v} = 0$
CII	$\hat{\mathbf{n}} \times [\mathbf{E} + \mathbf{v} \times \mathbf{B}]^+_- = \mathbf{0}$	$\hat{\mathbf{n}} \times [\eta\nabla \times \mathbf{B}]^+_- = \mathbf{0}$	Eqs. (2) and (5)

electric field $\mathbf{E}'$ measured in the frame moving with velocity $\mathbf{v}$ is related to that measured in the laboratory frame $\mathbf{E}$ via $\mathbf{E}' = \mathbf{E} + \mathbf{v} \times \mathbf{B}$, where $\mathbf{B}$ is the magnetic field, which has the same value in both frames, i.e., $\mathbf{B} = \mathbf{B}'$. A careful inspection of Maxwell's equations in the integral form shows that Eq. (1) should, in fact, read [5,6](see also [11])

$$\hat{\mathbf{n}} \times [\mathbf{E}']^+_- = \mathbf{0}$$
$$\Leftrightarrow \hat{\mathbf{n}} \times [\mathbf{E} + \mathbf{v} \times \mathbf{B}]^+_- = \mathbf{0}. \tag{2}$$

For convenience, we provide our own derivation of the above in the Appendix. Equations (1) and (2) are equivalent only when the two media are at rest relative to each other, i.e., when $[\mathbf{v}]^+_- = \mathbf{0}$. In particular, they are incompatible in situations where the two media are in *sliding contact*. In that case, Satapathy and Hsieh [12] recently demonstrated the validity of Eq. (2) based on two rail gun experiments. Nonetheless, Eq. (1) seems to be favored in most applications. A case in point is the experiment of Herzenberg and Lowes [13], who studied induction in a rotating cylinder permeated by a uniform magnetic field.

In the remainder of this section, we illustrate the difference between Eqs. (1) and (2) using a simple model resembling the experiment of Herzenberg and Lowes. For this purpose, we need the following additional condition, which is always true:

$$\hat{\mathbf{n}} \cdot [\mathbf{B}]^+_- = 0. \tag{3}$$

It will also be useful to rewrite Eqs. (1) and (2) to avoid explicit mentions of the electric field. Using *Ohm's law*, $\mathbf{j} = \sigma(\mathbf{E} + \mathbf{v} \times \mathbf{B})$, where $\mathbf{j}$ is the electric current density and σ is the electric conductivity, combined with *Ampère's law* in the pre-Maxwell form relevant in magnetohydrodynamics applications [1], $\nabla \times \mathbf{B} = \mu\mathbf{j}$, where μ is the magnetic permeability, Eq. (1) becomes

$$\hat{\mathbf{n}} \times [\eta\nabla \times \mathbf{B}]^+_- = (\hat{\mathbf{n}} \cdot \mathbf{B})[\mathbf{v}]^+_- - [(\hat{\mathbf{n}} \cdot \mathbf{v})\mathbf{B}]^+_-, \tag{4}$$

where we used Eq. (3) and we introduced the magnetic diffusivity $\eta \equiv (\sigma\mu)^{-1}$. In this work, we focus on the case where $(\hat{\mathbf{n}} \cdot \mathbf{v}) = 0$; that is, we take the boundary as static and impermeable to the velocity, allowing us to discard that last term in (4). By contrast, Eq. (2) reduces to

$$\hat{\mathbf{n}} \times [\eta\nabla \times \mathbf{B}]^+_- = \mathbf{0}. \tag{5}$$

Table I summarizes the interface conditions used throughout this work.

Finally, we also make use of the following definition of the surface current density $\mathbf{j}_s$ in terms of the tangential component of the magnetic field [6]:

$$\hat{\mathbf{n}} \times [\mathbf{B}/\mu]^+_- = \mathbf{j}_s. \tag{6}$$

B. Paradox: Induction in a solid cylinder

We focus on the simple model introduced by Moffatt [5] and shown in Fig. 1(a) (see also [14]). A cylindrical region filling the domain $s \in [0, R]$, with s being the cylindrical radial coordinate, rotates steadily around the z axis at the angular velocity Ω. The whole volume is permeated by a transverse uniform external magnetic field $\mathbf{B}_0$ along the x direction. For simplicity, we assume that the cylinder and surrounding space have equal magnetic diffusivities η. We solve the induction equation:

$$\partial_t \mathbf{B} = \nabla \times (\mathbf{v} \times \mathbf{B}) + \eta\nabla^2\mathbf{B}, \tag{7}$$

assuming $\partial_t \mathbf{B} = \mathbf{0}$ (steady regime). The system is then controlled by the value of the dimensionless *magnetic Reynolds number*, here defined as $\mathrm{Rm} \equiv \Omega R^2/\eta$. The solution for the magnetic field can be advantageously expressed as the real part of $\mathbf{B} = \nabla \times (A_z\hat{\mathbf{z}})$, with (see [5] for details)

$$A_z = B_0 e^{i\varphi} \begin{cases} c_1 J_1\big((1-i)\sqrt{\frac{\mathrm{Rm}}{2}}\frac{s}{R}\big), & s \leqslant R, \\ c_2 s^{-1} - s, & s > R, \end{cases} \tag{8}$$

where φ is the cylindrical azimuthal coordinate and J_n denotes the Bessel function of degree n. The two integration constants, c_1 and c_2, are determined by boundary conditions. Equation (3) yields a single relation between c_1 and c_2, and a second one is needed.

In the steady regime considered, $\mathbf{E} = \mathbf{0}$ both inside and outside of the cylinder, as can be checked readily with Eq. (8) combined with Ampère's and Ohm's laws. Condition CI therefore provides no constraint on the solution. In that same regime, it is then typical to consider that any surface currents at the interface have had ample time to diffuse into the volume such that, from Eq. (6), $\hat{\mathbf{n}} \times [\mathbf{B}]^+_- = \mathbf{0}$. One then finds

$$c_1 = -\frac{2R}{\xi J_0(\xi)}, \quad c_2 = R^2\left(1 - \frac{2J_1(\xi)}{\xi J_0(\xi)}\right), \tag{9}$$

where we have defined $\xi = (1-i)(\mathrm{Rm}/2)^{1/2}$. Figure 1(b) shows the corresponding solution for $\mathrm{Rm} = 10$. By contrast, condition CII *does* provide a constraint on the solution and leads to

$$c_1 = 0, \quad c_2 = R^2. \tag{10}$$

The corresponding solution is shown in Fig. 1(c). The most striking feature is the absence of magnetic induction inside the cylinder, which behaves as a perfect conductor [as confirmed by taking the limit $\mathrm{Rm} \to \infty$ in Eq. (9)] even though we made no assumption about the value of Rm in arriving at Eq. (10). This solution also implies the existence of surface currents, as can be seen by inserting it back into Eq. (6), a feature that seems unphysical in the steady regime.

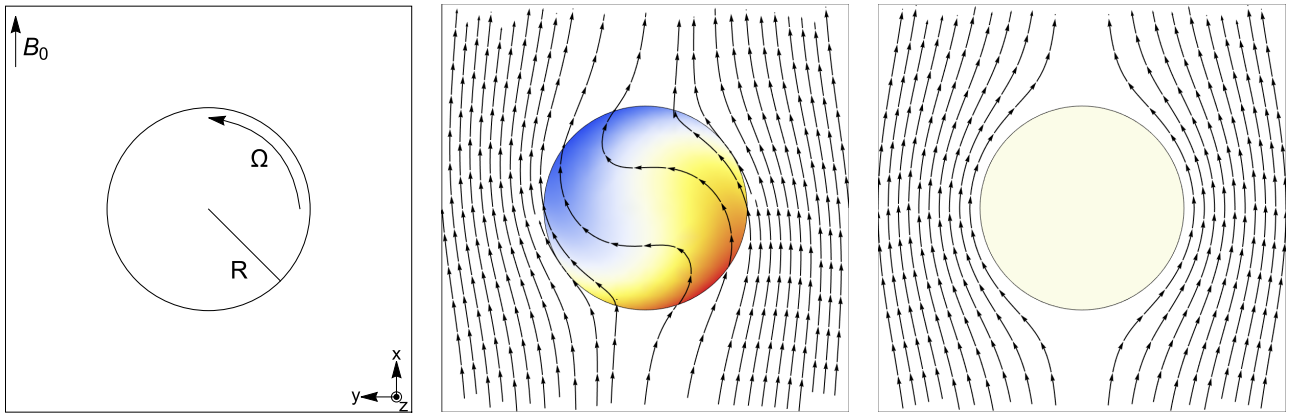

(a) Geometry (b) (C.I) and $\hat{\mathbf{n}} \times [\mathbf{B}]_-^+ = \mathbf{0}$ (c) (C.II) and $\hat{\mathbf{n}} \times [\mathbf{B}]_-^+ \neq \mathbf{0}$

FIG. 1. (a) A rotating cylinder is immersed within a transverse uniform background magnetic field. (b) Solution for Rm = 10, based on condition CI and assuming continuity of the tangent magnetic field at the boundary. Streamlines show the magnetic field; colors show the normalized value of the axial current density, with blue and red pointing, respectively, inside and outside the page. (c) Same as in (b), but based on condition CII and allowing for surface currents. The internal magnetic field is zero in that case for all values of Rm, and the current density is restricted to a vanishingly thin sheet at the cylinder's surface.

The inadequacy of condition CII to reproduce the experimental results of Herzenberg and Lowes can be traced back to the assumption that the rotating cylinder and its surroundings are in sliding contact. In the experiment, the cylinder maintains electric contact with its supporting apparatus via a very thin layer of mercury which also serves as a lubricant. Because of its finite viscosity, this intermediate layer becomes the host of intense shears during rotation. Section A 3 of the Appendix gives a formal derivation of the appropriate boundary condition in the presence of such a transition layer. In the following section we take a closer look at the role played by shears at the interface.

III. THE ROLE OF SHEAR AT THE INTERFACE

We consider the simple toy model depicted in Fig. 2 that represents the interface between two conducting rigid media. The whole volume is permeated by a uniform external magnetic field $\mathbf{B}_0$ pointing along the normal to the interface chosen z axis, and the upper medium oscillates tangentially at a prescribed frequency ω, so that the velocity is written as

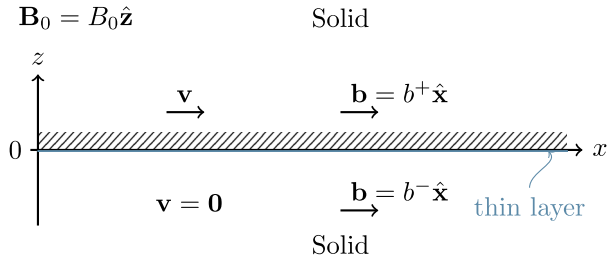

FIG. 2. Local model of the interface between two semi-infinite conducting solids sliding on top of each other. The presence of a thin viscous layer between the two solids (in blue) radically affects the solution (see the text).

$\mathbf{v} = v\hat{\mathbf{x}}$, with

$$v = \begin{cases} \mathrm{Re}[\tilde{v}e^{-i\omega t}], & z \geqslant 0, \\ 0, & z < 0. \end{cases} \tag{11}$$

For simplicity, we take the magnetic diffusivity to be constant in the whole volume. We also focus exclusively on the region near the interface, so that we can safely approximate both sides as semi-infinite. The total magnetic field is written as $\mathbf{B} = \mathbf{B}_0 + \mathbf{b}$, where $\mathbf{b}$ is the perturbation induced by the oscillations which must obey the induction (7). We first look at the case where the thin viscous layer (in blue in Fig. 2) is absent.

The induced field must point in the same direction as the velocity, and its magnitude can depend on only z because of symmetry. We thus write $\mathbf{b} = b\hat{\mathbf{x}}$, with

$$b = \begin{cases} \mathrm{Re}[\tilde{b}^+e^{i(\lambda^+z-\omega t)}], & z \geqslant 0, \\ \mathrm{Re}[\tilde{b}^-e^{i(\lambda^-z-\omega t)}], & z < 0. \end{cases} \tag{12}$$

We obtain λ^+ and λ^- by inserting the above into the induction (7) and imposing regularity of the solution at $z \to \pm\infty$, giving

$$\lambda^\pm = \pm\frac{1+i}{\delta_*}, \tag{13}$$

where $\delta_* = \sqrt{2\eta/\omega}$ is the *magnetic skin depth*.

Finally, the values of the constants, $\tilde{b}^+$ and $\tilde{b}^-$, depend on our choice of boundary conditions. In an attempt to make sense of the paradox in Sec. II B, when condition CII is imposed, we consider this condition first. In the present situation this gives the constraint

$$\tilde{b}^+ = -\tilde{b}^-. \tag{14}$$

Again, we see that the above equation strictly prohibits the continuity of the tangential magnetic field across the interface, except in the trivial case where $\tilde{b}^+ = \tilde{b}^- = 0$, and there is no induction between the two media. On the other hand, condition CI can be rewritten here as

$$[\eta\partial_z b + B_0 v]_-^+ = 0. \tag{15}$$

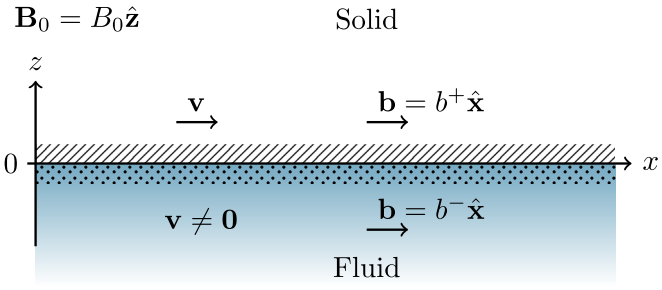

FIG. 3. Local model of the solid-fluid interface. The finite viscosity of the fluid causes the appearance of a thin boundary layer in the fluid region represented by the dotted area (see main text).

This condition combined with the requirement of zero surface current, $\tilde{b}^+ = \tilde{b}^-$, gives a nonzero value for the induced field on both sides:

$$\tilde{b}^{\pm} = (1+i)\frac{B_0\tilde{v}}{4\eta}\delta_*. \tag{16}$$

From the above, we see that condition CI is clearly incompatible with condition CII because they lead to very different solutions. Moreover, it would seem that the former should be preferred over the latter on empirical grounds, which is at odds with first principles, as well as plasma physics applications using condition CI. There is, however, a simple way to motivate the use of that condition physically if we consider the slightly modified situation where the thin blue intermediate viscous layer in Fig. 2 is present. We can model this by substituting the expression for the velocity (11) with one valid for the whole domain:

$$\mathbf{v} \to \Theta(z)\mathbf{v}, \tag{17}$$

where $\Theta(z)$ is the Heaviside distribution satisfying $\Theta(z \geqslant 0) = 1$ and $\Theta(z < 0) = 0$. Plugging the result into Eq. (7), keeping only linear terms in $\mathbf{v}$ and $\mathbf{b}$, and using the identity $d\Theta/dz = \delta(z)$ give

$$\partial_t\mathbf{b} = B_0\delta(z)\mathbf{v} + \eta\nabla^2\mathbf{b}, \tag{18}$$

where $\delta(z)$ is the Dirac distribution. Integrating Eq. (18) over an infinitesimal line segment across the interface (see [15]) gives back Eq. (15), from which Eq. (16) follows. This argument demonstrates the important role of viscous layers at the interface between two solids. It is valid as long as we can reasonably approximate that layer as infinitely thin but breaks down in situations where the conducting viscous fluid has a finite volume, to which we now turn.

IV. SHEAR LAYER AT A SOLID-FLUID INTERFACE

We consider the situation depicted in Fig. 3. It is analogous to that in Sec. III, except that the bottom region is now fluid and has finite viscosity. The flow velocity $\mathbf{v}$ in the fluid region is governed by the momentum equation:

$$\partial_t\mathbf{v} + (\mathbf{v}\cdot\nabla)\mathbf{v} = -\frac{\nabla P}{\rho} + \frac{1}{\rho\mu}(\nabla\times\mathbf{B})\times\mathbf{B} + \nu\nabla^2\mathbf{v}, \tag{19}$$

where ν is the kinematic viscosity, P is the pressure, and ρ is the mass density taken to be constant. $\mathbf{B}$ is the total magnetic field governed by the induction (7). We proceed as before

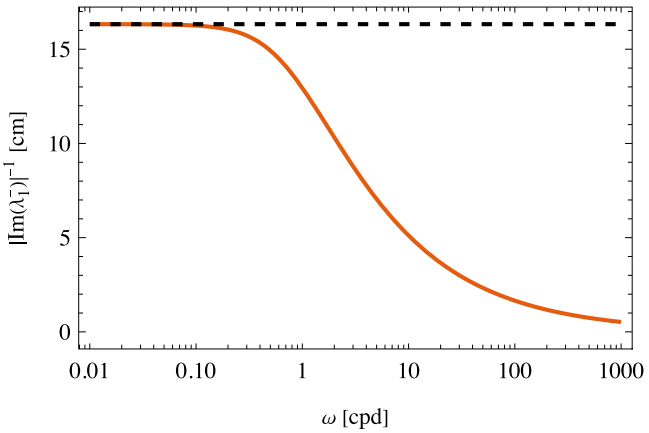

FIG. 4. Thickness of the boundary layer at the fluid-solid interface for parameters typical of Earth's upper fluid core as a function of the frequency (in cycles per day). The dashed line shows the steady limit corresponding to the Hartmann layer thickness $\delta_H = \sqrt{\nu\eta}/v_A$.

and write $\mathbf{B} = \mathbf{B}_0 + \mathbf{b}$. The magnetic perturbation assumes the same form as Eq. (12). The fluid velocity has a similar form but is limited to the fluid region, so the whole velocity field $\mathbf{v} = v\hat{\mathbf{x}}$ can be summarized as

$$v = \begin{cases} \mathrm{Re}[\tilde{v}^+ e^{-i\omega t}], & z \geqslant 0, \\ \mathrm{Re}[\tilde{v}^- e^{i(\lambda^- z - \omega t)}], & z < 0. \end{cases} \tag{20}$$

To linear order in $\mathbf{v}$ and $\mathbf{b}$, Eqs. (7) and (19) may then be written in the following matrix form:

$$\begin{pmatrix} v_A\lambda\sqrt{\rho\mu} & \omega + i\lambda^2\eta \\ \omega + i\lambda^2\nu & v_A\lambda/\sqrt{\rho\mu} \end{pmatrix}\begin{pmatrix} \tilde{b} \\ \tilde{v} \end{pmatrix} = 0, \tag{21}$$

where we have dropped the superscripts from $\tilde{v}^-$, $\tilde{b}^-$, and λ^- for readability and we have introduced $v_A = B_0/\sqrt{\rho\mu}$, representing the *Alfvén velocity* inside the fluid [16]. The determinant of the matrix in Eq. (21) must be equal to zero. Solving for λ, we find (see [17])

$$\lambda^2 = -\left(\frac{v_A^2}{2\eta\nu} - i\omega\frac{\eta+\nu}{2\eta\nu}\right) \pm \sqrt{\frac{\omega^2}{\eta\nu} - \left(\omega\frac{(\eta+\nu)}{2\eta\nu} + i\frac{v_A^2}{2\eta\nu}\right)^2}. \tag{22}$$

The numerical values of these numbers depend on the parameters. With geophysical applications in mind, we take values that are typical for Earth's core: $\rho = 10^4$ kg/m^3, $\mu = 4\pi\times10^{-7}$ H/m, $\eta = 0.5$ m^2/s, $\nu = 10^{-6}$ m^2/s, and $v_A = 4.5\times10^{-3}$ m/s.

In total, there are four solutions for λ which we parametrize as (reintroducing the superscript)

$$\lambda^- = k - i\delta^{-1}, \tag{23}$$

where k and δ are real numbers representing the wave number and the decay length, respectively. We keep only solutions satisfying $\delta > 0$, which ensures that the perturbations converge to zero at $z \to -\infty$. Among the two remaining solutions, there is one for which k is large and δ is small, representing a rapidly decaying short wavelength plane wave. For the other,

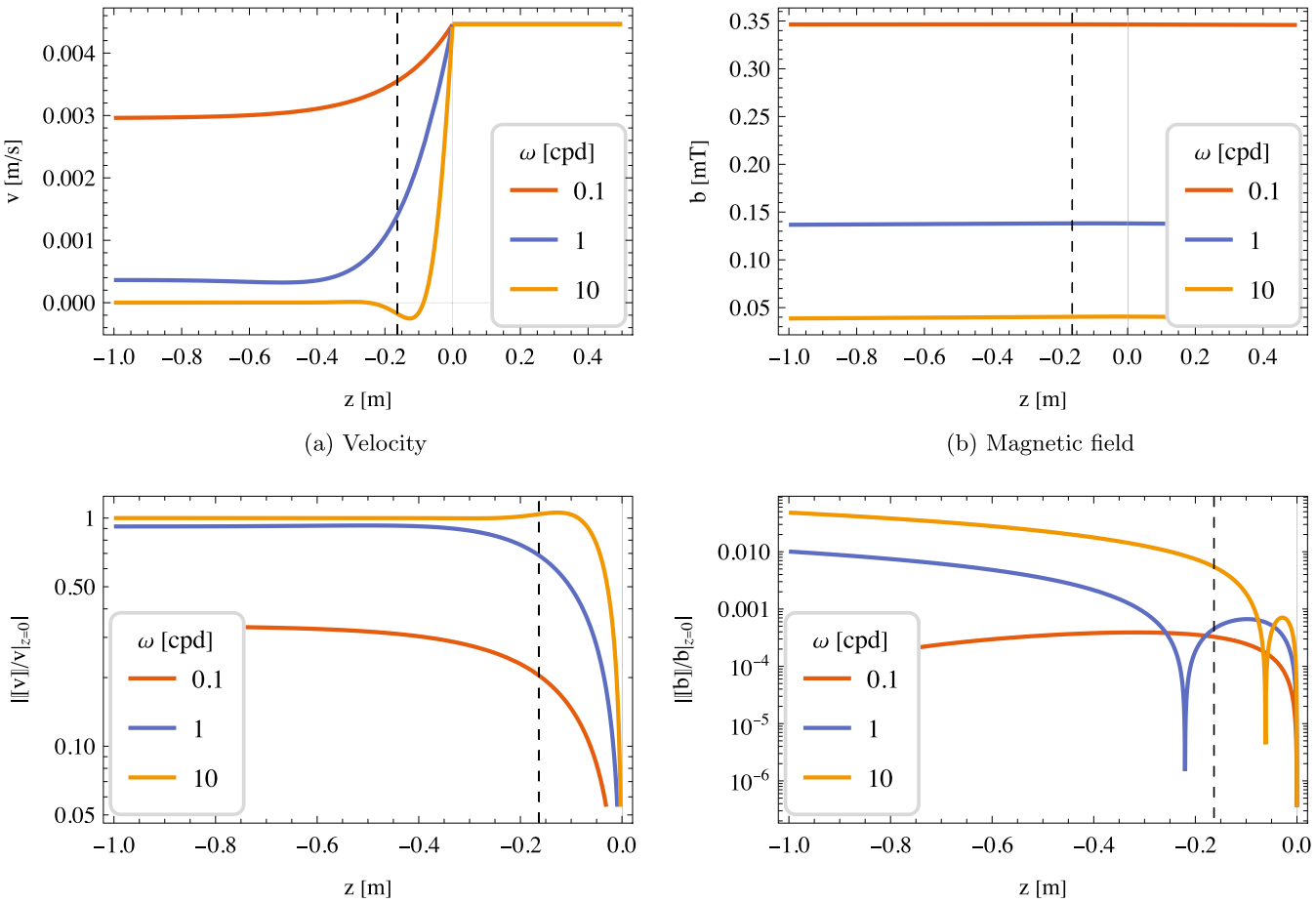

(a) Velocity (b) Magnetic field

(c) Jump in velocity (d) Jump in magnetic field

FIG. 5. Top: velocity and magnetic field perturbations as a function of depth for three values of the frequency (in cycles per day). Bottom: relative jump in velocity and magnetic field. The black dashed lines indicate the depth of the Hartmann layer in the steady limit (see Fig. 4).

k is small, and δ is large, representing a slowly decaying plane wave with long wavelength:

$$\text{Boundary layer:} \quad \{\tilde{v}_1^-, \tilde{b}_1^-\}, \quad \lambda_1^- = k_1 - i\delta_1^{-1}, \tag{24a}$$

$$\text{Traveling wave:} \quad \{\tilde{v}_2^-, \tilde{b}_2^-\}, \quad \lambda_2^- = k_2 - i\delta_2^{-1}, \tag{24b}$$

with $\delta_1 \ll \delta_2$ and $k_1 \gg k_2$. In the first solution, δ_1 corresponds to the thickness of the boundary layer illustrated by the dotted area in Fig. 3. Its thickness is shown in Fig. 4 as a function of the frequency, given in cycles per day (cpd). It is maximum in the steady limit, where it is equal to the *Hartmann layer* thickness $\delta_H = \sqrt{\nu\eta}/v_A$ (dashed line). Like for the solid interface, the constants $\tilde{v}_1^-$, $\tilde{b}_1^-$, $\tilde{v}_2^-$, and $\tilde{b}_2^-$, as well as $\tilde{b}^+$ for the upper solid region, are set by the boundary conditions. The values of $\tilde{b}_1^-$ and $\tilde{b}_2^-$ are related to $\tilde{v}_1^-$ and $\tilde{v}_2^-$ by Eq. (21), so that only three constraints are needed. One is given by the requirement that the velocity be continuous across the interface (no slip). This renders the condition on the tangential electric field unambiguous, the latter serving as our second constraint. Finally, we assume that the tangential magnetic field is continuous at the interface (no surface currents). In our simple model, these three constraints are written as

$$\text{No slip:} \quad \tilde{v}_1^- + \tilde{v}_2^- = \tilde{v}^+, \tag{25a}$$

$$\text{Current continuity, CI and CII are equivalent:} \quad \lambda_1^-\tilde{b}_1^- + \lambda_2^-\tilde{b}_2^- = \lambda^+\tilde{b}^+, \tag{25b}$$

$$\text{Magnetic field continuity:} \quad \tilde{b}_1^- + \tilde{b}_2^- = \tilde{b}^+. \tag{25c}$$

The solution is then completely determined once we set the value of $\tilde{v}^+$. For simplicity, we take $\tilde{v}^+ = v_A$, which matches well the relative velocity between Earth's core and mantle induced by Earth's precession [18].

Figures 5(a) and 5(b) show the magnitude of the velocity and magnetic field as a function of depth for three values of the frequency. The vertical dashed line on each plot indicates the width of the Hartmann layer in the steady limit (see Fig. 4).

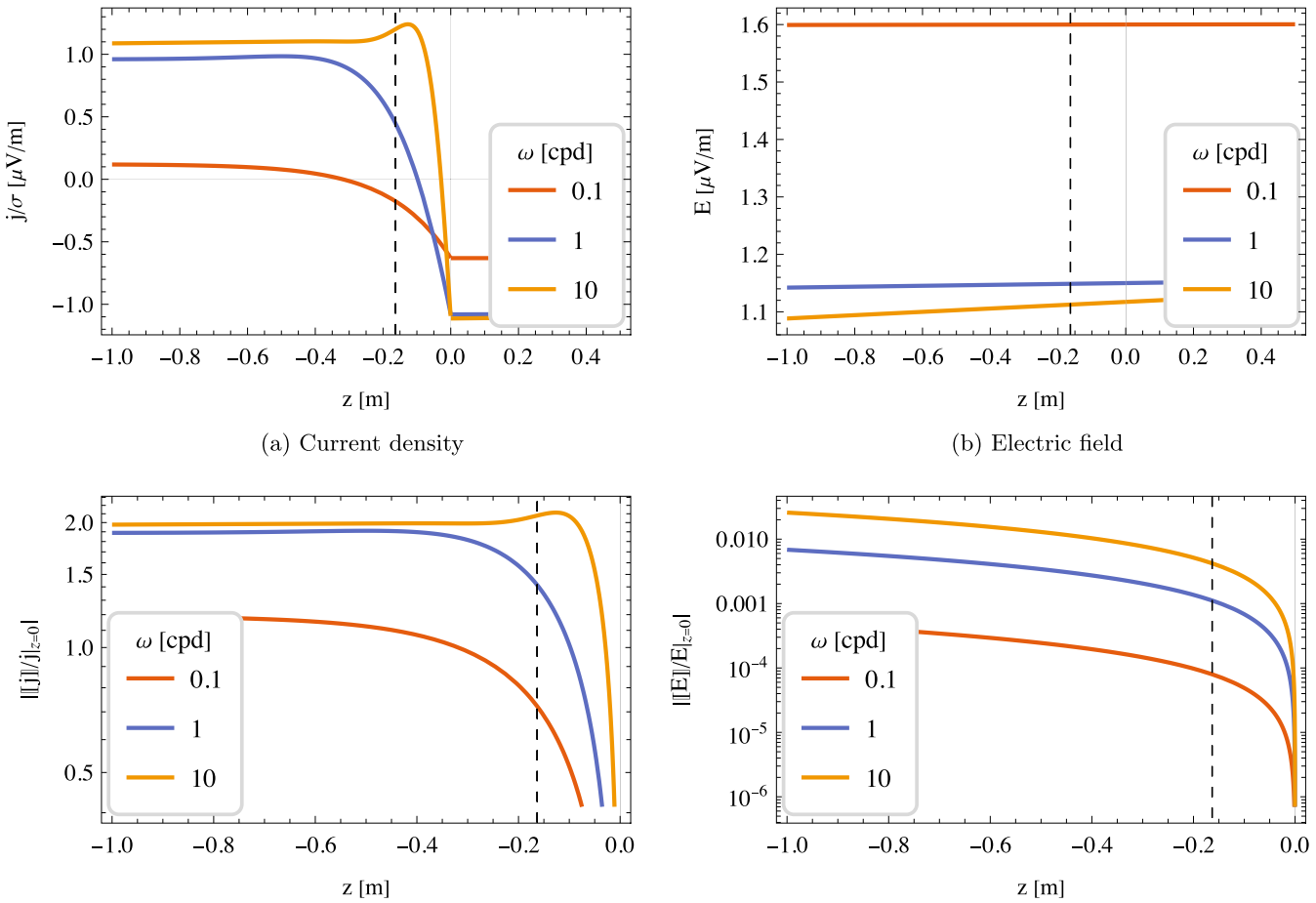

(a) Current density (b) Electric field

(c) Jump in current density (d) Jump in electric field

FIG. 6. Top: electric current density divided by electric conductivity and electric field near the interface. Bottom: relative jump in current density and electric field. The black dashed lines indicate the depth of the Hartmann layer in the steady limit (see Fig. 4).

While the effect of this boundary layer is clearly visible on the velocity profile, it is hardly discernible in the magnetic field perturbation. This is the expected behavior for fluids with $\eta \gg \nu$, such as in Earth's core [19,20]. In this case, the velocity of the flow just below the boundary layer converges quickly to its value in the bulk of the fluid—the so-called *free stream*—which is here simply $v = 0$. In order to better quantify changes across the boundary layer, we introduce the following notation (see [21,22]):

$$[[b]] \equiv b|_{z=0} - b, \tag{26}$$

with similar notation for v and other quantities. The jumps in v and b are shown in Figs. 5(c) and 5(d) as a function of depth, in absolute value and normalized by the values of those fields at the interface.

Finally, we can use our simple toy model to probe whether condition CI or CII better represents the behavior of the electric field near the interface. Figures 6(a) and 6(b) show the magnitude of the electric current density divided by the electric conductivity, $\mathbf{j}/\sigma = \mathbf{E} + \mathbf{v} \times \mathbf{B}_0$, and of the electric field $\mathbf{E}$ as a function of depth for three values of the frequency. Figures 6(c) and 6(d) show the jump in these quantities divided by their values at the interface. We can see that the current density varies a lot across the boundary layer, whereas the electric field remains almost constant. We can express this mathematically as

$$[[\eta \partial_z b + B_0 v]] \approx 0, \tag{27}$$

which is valid within the boundary layer. Equation (27) is analogous to Eq. (15) derived in Sec. III for the viscous solid-solid interface, which we found to be equivalent to condition CI. In this light, the latter can be perceived as the limit case of Eq. (27) when the boundary layer is infinitely thin. This result proves the validity of condition CI at a solid-fluid interface when it is understood as a condition relating the values of the fields inside the solid layer to their values at the top of the free stream, i.e., just below the thin boundary layer.

As we argued in Sec. III, condition CI automatically accounts for viscous shears at the interface and their effect on the fields. We can check that this is also true for the solid-fluid interface by slightly altering the above model, replacing the continuity (no-slip) condition on the velocity field at the interface with the condition on its gradient: $[\partial_z v]^+_- = 0$, which amounts to imposing that the shear stresses are continuous across the interface. As the upper medium is here assumed to

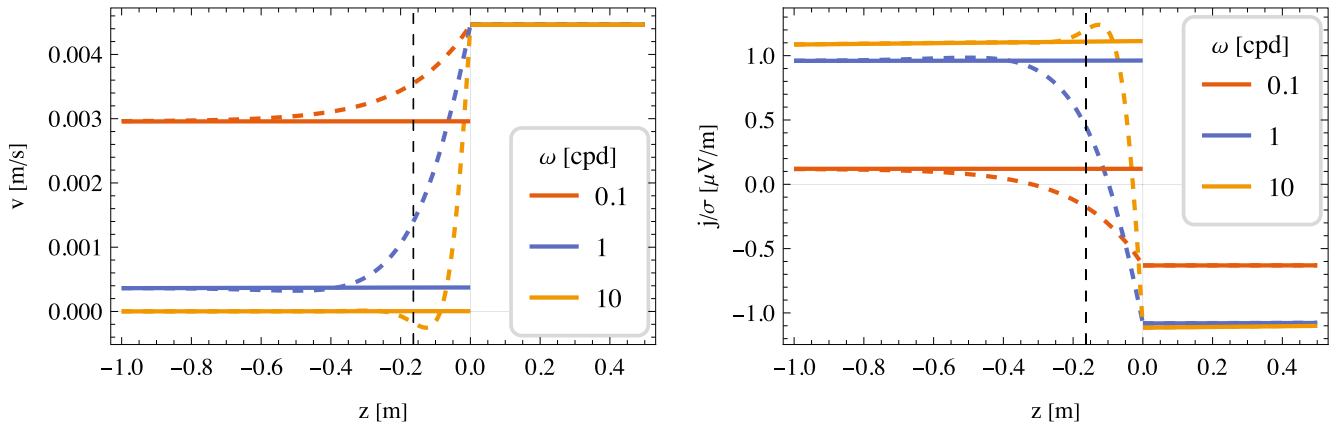

(a) Velocity (b) Current density

FIG. 7. Velocity and electric current density near a solid-fluid interface using the boundary conditions (28a) and (28b) (solid curves) compared to the exact solution in Sec. IV (dashed curves).

be perfectly rigid, the viscous stresses in the fluid must vanish at the boundary; this is the so-called *stress-free* condition. More specifically, this amounts to replacing Eqs. (25a) and (25b) by

$$\text{Stress free:} \qquad \lambda_1^- \tilde{v}_1^- + \lambda_2^- \tilde{v}_2^- = 0, \tag{28a}$$

$$\text{Electric field continuity (condition CI):} \qquad \eta(\lambda_1^- \tilde{b}_1^- + \lambda_2^- \tilde{b}_2^- - \lambda^+ \tilde{b}^+) = iB_0(v_1^- + v_2^- - v^+), \tag{28b}$$

with Eq. (32) reducing to Eq. (25b) only in the no-slip hypothesis. Figure 7 shows the solution for v and the magnitude of $\mathbf{j}/\sigma$ using Eqs. (28a) and (28b). The dashed curves correspond to the exact solution of Sec. IV given for comparison. We see that, even though shears have been removed from the model, the exact solution rapidly becomes equivalent to the approximate solution outside of the boundary layer by virtue of condition CI alone. The approximate magnetic and electric fields are undistinguishable from the exact profiles shown in Figs. 5(b) and 6(b) and are therefore not repeated here.

V. CONCLUSION

The continuity condition on the tangential part of the electric field at the interface between two media depends on the details of the problem. In situations where the two sides are in true sliding contact, theoretical as well as experimental considerations indicate that condition CII should be preferred over condition CI. We have shown how the latter becomes relevant whenever an intermediary viscous layer is present between the two media. For a solid-fluid interface, this layer corresponds to the fluid boundary layer. Therefore, both geophysical and plasma physics applications (just to name a few) are equally justified in their respective usage of conditions CI and CII, with the former operating under the often implicit assumption that there are boundary layers present.

In practical fluid dynamics computations, the very small thickness of such layers can be challenging to model. This is certainly true when dealing with Earth's fluid core, in which case it is sometimes useful to get rid of the boundary layer entirely by assuming that the free stream extends all the way to the interface, thereby approximating the sharp jump in the flow velocity at the interface as a true discontinuity. In that case, we showed in Sec. IV that using condition CI guarantees that the approximate solution will be close to the physical solution if the boundary layer of the latter is sufficiently thin (Fig. 7), even though the use of condition CI is not strictly self-consistent from a theoretical point of view.

In summary, in order to decide which condition to use in a given application, one should start by assessing the presence and thickness of viscous layers at the interface considered. This assessment and its consequences for practical studies of the magnetohydrodynamics of Earth's fluid core will be presented in a future work.

ACKNOWLEDGMENTS

J.R. and S.A.T. express their warm gratitude to V. Dehant and T. Van Hoolst for their encouragement and support, as well as F. Gerick for enriching discussions. The research leading to these results has received funding from the European Research Council (ERC) under the European Union's Horizon 2020 research and innovation program (Synergy Grant Agreement No. 855677 GRACEFUL). J.R. would like to thank the University of California, Berkeley's Department of Earth and Planetary Science for their hospitality during the making of this work. We would also like to thank the anonymous reviewer for their comments, which helped to improve some of the arguments presented in the original manuscript.

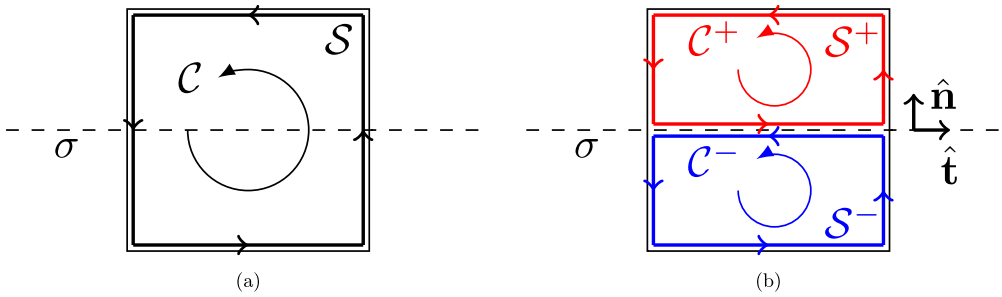

FIG. 8. (a) The circuit contour $\mathcal{C}$ enclosing the surface $\mathcal{S}$ intersects the surface of discontinuity between two regions of space perpendicularly along the straight line σ. (b) It is always possible to decompose each of $\mathcal{C}$ and $\mathcal{S}$ into two parts if we specify appropriate junction conditions at σ (see the text).

APPENDIX: DERIVATION OF THE ELECTRIC BOUNDARY CONDITION

1. Faraday's law of induction

Faraday's law of induction is related to the rate of change of the magnetic field flux through the (open) surface $\mathcal{S}$ to the *electromotive force*, acting on that surface, with the latter being defined as the integral of the *Lorentz force* per unit charge over the enclosing contour $\mathcal{C}$:

$$-\frac{d}{dt}\int_{\mathcal{S}(t)} \mathbf{B}\cdot\hat{\boldsymbol{n}}dS = \oint_{\mathcal{C}(t)} (\mathbf{E}+\mathbf{v}\times\mathbf{B})\cdot\hat{\boldsymbol{t}}dl, \tag{A1}$$

where $\hat{\boldsymbol{n}}$ and $\hat{\boldsymbol{t}}$ denote the unit vectors normal to $\mathcal{S}$ and tangent to $\mathcal{C}$, respectively. In general, these two domains may be time dependent, as reflected in the above notation. This prevents simply swapping the order of the integral and time derivative in Eq. (A1). Instead we have, based on *Reynolds's transport theorem* (see, e.g., [23]),

$$-\frac{d}{dt}\int_{\mathcal{S}(t)} \mathbf{B}\cdot\hat{\boldsymbol{n}}dS = -\int_{\mathcal{S}(t)} \left(\frac{\partial\mathbf{B}}{\partial t} + (\nabla\cdot\mathbf{B})\mathbf{v}\right)\cdot\hat{\boldsymbol{n}}dS + \oint_{\mathcal{C}(t)} (\mathbf{v}\times\mathbf{B})\cdot\hat{\boldsymbol{t}}dl. \tag{A2}$$

Inserting the result back into Eq. (A1) and using $\nabla\cdot\mathbf{B}=0$, we find

$$-\int_{\mathcal{S}(t)} \frac{\partial\mathbf{B}}{\partial t}\cdot\hat{\boldsymbol{n}}dS = \oint_{\mathcal{C}(t)} \mathbf{E}\cdot\hat{\boldsymbol{t}}dl. \tag{A3}$$

At this point, we must emphasize that Eq. (A2) is valid only if *both* $\mathbf{B}$ and $\mathbf{v}$ are differentiable functions throughout the surface $\mathcal{S}$. If, in addition, the electric field $\mathbf{E}$ is *continuous* throughout the same surface, we may use *Stokes's theorem*, which in the present context reads

$$\oint_{\mathcal{C}(t)} \mathbf{E}\cdot\hat{\boldsymbol{t}}dl = \int_{\mathcal{S}(t)} \nabla\times\mathbf{E}\cdot\hat{\boldsymbol{n}}dS. \tag{A4}$$

Combining Eqs. (A3) and (A4), we finally arrive at

$$\int_{\mathcal{S}(t)} \left(\frac{\partial\mathbf{B}}{\partial t} + \nabla\times\mathbf{E}\right)\cdot\hat{\boldsymbol{n}}dS = \mathbf{0}. \tag{A5}$$

The above must be valid for any surface $\mathcal{S}(t)$, which implies that

$$\nabla\times\mathbf{E} = -\frac{\partial\mathbf{B}}{\partial t}, \tag{A6}$$

which is one of *Maxwell's equations* in the local (differential) form. Crucially, the above derivation shows that Eq. (A6) is independent of the reference frame. It also explains why it would be inconsistent to try to replace $\mathbf{E}$ by $\mathbf{E}+\mathbf{v}\times\mathbf{B}$ in the above equation. Doing so would miss the effect induced by the motion of the surface element that is implicit in Eq. (A6) but explicit in Eq. (A1). This makes the latter generally more suited for deriving boundary conditions.

2. Electric boundary condition

In the previous section, we assumed that the three vectors $\mathbf{v}$, $\mathbf{B}$, and $\mathbf{E}$ are continuous throughout the whole domain. We now look at what happens when this is not the case by considering the situation in Fig. 8(a), where the surface $\mathcal{S}$ intersects the interface between two regions of space perpendicularly along the dashed line σ with unit normal and tangent vectors $\hat{\mathbf{n}}$ and $\hat{\mathbf{t}}$, which should not be confused with the previously introduced "dummy" vector variables $\hat{\boldsymbol{n}}$ and $\hat{\boldsymbol{t}}$. If $\mathbf{v}$, $\mathbf{B}$, and $\mathbf{E}$ are *piecewise* continuous on both sides of the surface, we can do as in Fig. 8(b) and divide the surface $\mathcal{S}$ into two parts, $\mathcal{S}^+$ and $\mathcal{S}^-$, such that $\mathcal{S}=\mathcal{S}^+\cup\mathcal{S}^-$, and we have the following property:

$$\int_{\mathcal{S}} \mathbf{A}\cdot\hat{\boldsymbol{n}}dS = \int_{\mathcal{S}^+} \mathbf{A}^+\cdot\hat{\boldsymbol{n}}dS + \int_{\mathcal{S}^-} \mathbf{A}^+\cdot\hat{\boldsymbol{n}}dS, \tag{A7}$$

which is true for any vector $\mathbf{A}$ that is piecewise continuous on $\mathcal{S}^+$ and $\mathcal{S}^-$, where its value is denoted formally as $\mathbf{A}^+$ and $\mathbf{A}^-$, respectively. We have to be a little more careful in combining contour integrals [24]:

$$\oint_{\mathcal{C}} \mathbf{A}\cdot\hat{\boldsymbol{t}}dl = \oint_{\mathcal{C}^+} \mathbf{A}^+\cdot\hat{\boldsymbol{t}}dl + \oint_{\mathcal{C}^-} \mathbf{A}^-\cdot\hat{\boldsymbol{t}}dl - \int_{\sigma} [\mathbf{A}]^+_-\cdot\hat{\mathbf{t}}dl, \tag{A8}$$

where we have replaced $\hat{\boldsymbol{t}}$ by its constant value, $\hat{\mathbf{t}}$, in the last term, as shown in Fig. 8(b), and we have used the following notation introduced in the main text:

$$[\mathbf{A}]^+_- \equiv (\mathbf{A}^+ - \mathbf{A}^-)|_\sigma. \tag{A9}$$

In the special case where $\mathbf{A}$ is continuous throughout the whole domain, the two values, $\mathbf{A}^+$ and $\mathbf{A}^-$, converge to a single limit at σ, and the last term in Eq. (A8) is zero.

Inserting Eqs. (A7) and (A8) into Faraday's law (A1), we may then repeat the exercise in the previous section to reduce

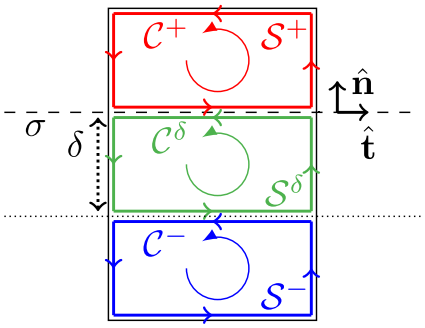

FIG. 9. Similar to Fig. 8(b), but with an intermediate transition layer of thickness δ with cross section $\mathcal{S}^\delta$ enclosed by the contour $\mathcal{C}^\delta$.

the contour integrals on both sides of the interface into surface integrals which may then be combined into a single integral using Eq. (A7). The final result is

$$\int_{\mathcal{S}(t)} \left(\frac{\partial \mathbf{B}}{\partial t} + \nabla \times \mathbf{E} \right) \cdot \hat{\boldsymbol{n}} dS = \int_\sigma [\mathbf{E} + \mathbf{v} \times \mathbf{B}]_-^+ \cdot \hat{\mathbf{t}} dl. \tag{A10}$$

Equation (A10) must be valid regardless of our choice of surface $\mathcal{S}$. In particular, taking the limit $\mathcal{S} \to 0$, we must have

$$[\mathbf{E} + \mathbf{v} \times \mathbf{B}]_-^+ \cdot \hat{\mathbf{t}} = 0, \tag{A11}$$

which is equivalent to condition CII.

3. Electric boundary condition with a transition layer

We now turn to the situation represented in Fig. 9, where, in addition to the two regions $\mathcal{S}^+$ and $\mathcal{S}^-$, there is an intermediate region of width δ with cross section $\mathcal{S}^\delta$ enclosed by the contour $\mathcal{C}^\delta$, within which the values of all fields transition smoothly between those of $\mathcal{S}^+$ and $\mathcal{S}^-$ so that the fields are continuous everywhere. We may thus write $\mathcal{S} = \mathcal{S}^+ \cup \mathcal{S}^\delta \cup \mathcal{S}^-$, and in analogy to Eqs. (A7) and (A8), we have

$$\int_{\mathcal{S}} \mathbf{A} \cdot \hat{\boldsymbol{n}} dS = \int_{\mathcal{S}^+} \mathbf{A}^+ \cdot \hat{\boldsymbol{n}} dS + \int_{\mathcal{S}^-} \mathbf{A}^+ \cdot \hat{\boldsymbol{n}} dS + \int_{\mathcal{S}^\delta} \mathbf{A}^\delta \cdot \hat{\boldsymbol{n}} dS, \tag{A12}$$

$$\oint_{\mathcal{C}} \mathbf{A} \cdot \hat{\boldsymbol{t}} dl = \oint_{\mathcal{C}^+} \mathbf{A}^+ \cdot \hat{\boldsymbol{t}} dl + \oint_{\mathcal{C}^-} \mathbf{A}^- \cdot \hat{\boldsymbol{t}} dl + \oint_{\mathcal{C}^\delta} \mathbf{A}^\delta \cdot \hat{\boldsymbol{t}} dl. \tag{A13}$$

Note that there is no boundary term analogous to the last one in Eq. (A8) in Eq. (A13) as we have assumed that $\mathbf{A}$ is continuous everywhere. Inserting the above equations into Faraday's law (A1), we may use Reynolds's theorem in all three regions in combination with Eq. (A12) to arrive at

$$-\int_{\mathcal{S}(t)} \frac{\partial \mathbf{B}}{\partial t} \cdot \hat{\boldsymbol{n}} dS = \oint_{\mathcal{C}^+(t)} \mathbf{E}^+ \cdot \hat{\boldsymbol{t}} dl + \oint_{\mathcal{C}^-(t)} \mathbf{E}^- \cdot \hat{\boldsymbol{t}} dl + \oint_{\mathcal{C}^\delta(t)} \mathbf{E}^\delta \cdot \hat{\boldsymbol{t}} dl. \tag{A14}$$

If, at this point, we assume that the intermediate transition region is very thin, corresponding to the limit $\delta \to 0$, the last term in Eq. (A14) goes to zero. Then, in order to combine the two remaining contour integrals on the right-hand side, we must use the formula in Eq. (A8) to account for a possible discontinuity of $\mathbf{E}$ at the junction between the two regions which, in the limit $\delta \to 0$, is located at σ. Using Stokes's theorem, we arrive at

$$\int_{\mathcal{S}(t)} \left(\frac{\partial \mathbf{B}}{\partial t} + \nabla \times \mathbf{E} \right) \cdot \hat{\boldsymbol{n}} dS = \int_\sigma [\mathbf{E}]_-^+ \cdot \hat{\mathbf{t}} dl, \tag{A15}$$

where we have again replaced $\hat{\boldsymbol{t}}$ by its constant value $\hat{\mathbf{t}}$. By analogy with Eq. (A10), we see that Eq. (A15) implies that

$$[\mathbf{E}]_-^+ \cdot \hat{\mathbf{t}} = 0, \tag{A16}$$

which is equivalent to condition CI.

[1] J. D. Jackson, *Classical Electrodynamics*, 3rd ed. (Wiley, New York, 1999).

[2] D. J. Griffiths, *Introduction to Electrodynamics*, 4th ed. (Pearson, Boston, 2013).

[3] R. P. Feynman, *The Feynman Lectures on Physics: Mainly Electromagnetism and Matter* (Addison-Wesley, Reading, Massachusetts, 1977), Vol. 2.

[4] M. Lax and D. F. Nelson, Maxwell equations in material form, Phys. Rev. B **13**, 1777 (1976).

[5] H. K. Moffatt, *Magnetic Field Generation in Electrically Conducting Fluids* (Cambridge University Press, Cambridge, 1978).

[6] A. C. Eringen and G. A. Maugin, *Electrodynamics of Continua. 1: Foundations and Solid Media* (Springer, New York, 1990).

[7] D. F. Nelson and M. Lax, Linear elasticity and piezoelectricity in pyroelectrics, Phys. Rev. B **13**, 1785 (1976).

[8] I. B. Bernstein, E. A. Frieman, M. D. Kruskal, R. M. Kulsrud, and S. Chandrasekhar, An energy principle for hydromagnetic stability problems, Proc. R. Soc. London, Ser. A **244**, 17 (1958).

[9] B. Lehnert, Plasma boundary conditions in an external magnetic field, Fusion Plasma Physics Alfven Laboratory, Technical Report No. TRITA-ALF-1997-02, 1997 (unpublished).

[10] D. D. Schnack, *Lectures in Magnetohydrodynamic*, Lecture Notes in Physics Vol. 780 (Springer, Berlin, 2009).

[11] K. S. Thorne and R. D. Blandford, *Modern Classical Physics: Optics, Fluids, Plasmas, Elasticity, Relativity, and Statistical Physics* (Princeton University Press, Princeton, NJ, 2017).

[12] S. Satapathy and K. Hsieh, Jump conditions for Maxwell equations and their consequences, AIP Adv. **3**, 012120 (2013).

[13] A. Herzenberg and F. J. Lowes, Electromagnetic induction in rotating conductors, Philos. Trans. R. Soc. London, Ser. A **249**, 507 (1957).

[14] P. A. Davidson, *An Introduction to Magnetohydrodynamics* (Cambridge University Press, Cambridge, 2001).

[15] B. A. Buffett, Constraints on magnetic energy and mantle conductivity from the forced nutations of the Earth, J. Geophys. Res. **97**, 19581 (1992).

[16] H. Alfvén, Existence of electromagnetic-hydrodynamic waves, Nature (London) **150**, 405 (1942).

[17] N. Schaeffer, D. Jault, P. Cardin, and M. Drouard, On the reflection of Alfvén waves and its implication for Earth's core modelling, Geophys. J. Int. **191**, 508 (2012).

[18] A. Tilgner, Rotational dynamics of the core, in *Treatise on Geophysics* (Elsevier, Amsterdam, Netherlands, 2015), pp. 183–212.

[19] K. Stewartson, Motion of bodies through conducting fluids, Rev. Mod. Phys. **32**, 855 (1960).

[20] K. Stewartson, On the motion of a non-conducting body through a perfectly conducting fluid, J. Fluid Mech. **8**, 82 (1960).

[21] P. H. Roberts and S. Scott, On analysis of the secular variation, J. Geomagn. Geoelectr. **17**, 137 (1965).

[22] D. J. Acheson and R. Hide, Hydromagnetics of rotating fluids, Rep. Prog. Phys. **36**, 159 (1973).

[23] R. Aris, *Vectors, Tensors and the Basic Equations of Fluid Mechanics*, Dover Books on Mathematics (Dover, New York, 1990).

[24] A. Eringen, *Mechanics of Continua* (Krieger, New York, 1980).